Center Vortices and Chiral Symmetry Breaking in $SU(2)$ Lattice Gauge Theory

Roman Höllwieser[a],[†] Thomas Schweigler, and Manfried Faber[‡]
Institute of Atomic and Subatomic Physics, Vienna University of Technology, Operngasse 9, 1040 Vienna, Austria

Urs M. Heller
American Physical Society, One Research Road, Ridge, NY 11961, USA

(Dated: April 5, 2013)

We investigate the chiral properties of near-zero modes for thick classical center vortices. In particular we analyze the creation of near-zero modes from would-be zero modes of various topological charge contributions from center vortices. We show that colorful spherical vortex and instanton ensembles have very similar Dirac eigenmodes and also vortex intersections are able to give rise to a finite density of near-zero modes, leading to chiral symmetry breaking via the Banks-Casher formula. We discuss the influence of the magnetic vortex fluxes on quarks and how center vortices may break chiral symmetry.

PACS numbers: 11.15.Ha, 12.38.Gc

[a] Funded by the Austrian Science Fund FWF ("Fonds zur Förderung der wissenschaftlichen Forschung") under Contract No. P22270-N16.
[†] hroman@kph.tuwien.ac.at
[‡] faber@kph.tuwien.ac.at

I. INTRODUCTION

Quantum chromodynamics (QCD) at low energies is dominated by the nonperturbative phenomena of quark confinement and spontaneous chiral symmetry breaking (χSB). Presently, a rigorous treatment of them is only possible in the lattice regularization. Many of the important features of non-Abelian gauge theories are already present in SU(2), which simplifies theoretical and numerical calculations.

The nonperturbative vacuum can be characterized by various kinds of topological gauge field excitations. A well established theory of χSB relies on instantons [1–4], which are localized in space-time and carry a topological charge of modulus 1. According to the Atiyah-Singer index theorem [5–8], a zero mode of the Dirac operator arises, which is concentrated at the instanton core. In the instanton liquid model [9–11] overlapping would-be zero modes split into low-lying nonzero modes which create the chiral condensate.

Center vortices [12–17], on the other hand, are promising candidates for explaining confinement. They form closed magnetic flux tubes, whose flux is quantized, taking only values in the center of the gauge group. These properties are the key ingredients in the vortex model of confinement, which is theoretically appealing and was also confirmed by a multitude of numerical calculations, *e.g.* [18, 19]. Lattice simulations indicate that vortices may be responsible for topological charge and χSB as well [20–25], and thus unify all nonperturbative phenomena in a common framework. A similar picture to the instanton liquid model exists insofar as lumps of topological charge arise at the intersection and writhing points of vortices. The colorful, spherical SU(2) vortex as introduced in previous articles of our group [26–29], may act as a prototype for this picture, as it contributes to the topological charge by its color structure, attracting a zero mode like an instanton.

In this article we want to show how the interplay of various topological structures from center vortices (and instantons) leads to near-zero modes. Using the overlap and asqtad staggered Dirac operator, we compute a varying number of the lowest-lying Dirac eigenfunctions, including the zero modes. By visualizing the probability density, we compare the distribution of the eigenmode density with the position of the vortices and the topological charge created by intersection points and color structures. These results manifest the importance of center vortices also for chiral symmetry breaking.

II. TOPOLOGICAL CHARGE FROM CENTER VORTICES

From the definition

$$Q \propto \epsilon_{\mu\nu\alpha\beta} F_{\mu\nu} F_{\alpha\beta} \,, \tag{1}$$

it is clear that topological charge contributions arise where two perpendicular nontrivial plaquettes meet. On a center vortex, the vortex sheet is locally orthogonal to the nontrivial plaquettes. Hence, topological charge emerges at so-called singular points of center vortices, where the set of tangent vectors to the vortex surface spans all four space-time directions [30]. There are two possibilities where this can occur:

- intersection points of two different surface patches: $Q = \pm 1/2$,
- writhing points of a single surface patch: $|Q| < 1/2$.

In lattice language, intersection points have four plaquettes attached to them extending in two particular space time directions (*e.g.* xy), and another four plaquettes extending in the two orthogonal directions (*e.g.* zt). By contrast, at a writhing point one can start at any attached plaquette and pass around over all others along a continuous path since they are connected by common links.

In SU(2), a Wilson loop cannot distinguish between center fluxes of opposite sign, since $\exp(i\pi) = \exp(-i\pi) = -1$. However, the sign of the topological charge is sensitive to the direction of the flux. To preserve this information for thin vortices, one can assign an orientation to the vortex patches. Note that this quantity is not directly linked to the geometry of the vortex. A nonorientable vortex need not be nonorientable as a surface [31].

Vortices always have closed surfaces. Furthermore, lattice studies show that the major fraction of vortex patches belongs to a single large vortex winding through the whole lattice. Intersections between different vortices are therefore only of minor importance. But for a closed oriented surface the total charge is zero. Charged vortices must therefore be globally nonoriented and consist of differently oriented patches, which are separated by monopole worldlines. The colorful spherical vortex is a classical representation of such a vortex configuration, contributing to topological charge only through its color structure. It will be discussed shortly in Sec. II B, but first let us explain the relation between vortices and magnetic monopoles, thereby making precise the definition of the orientation of a vortex.

On the lattice, monopoles are located by so-called Abelian projection. First, one fixes the links up to a residual $U(1)$-symmetry, which corresponds to an Abelian gauge theory. For example, we can use the maximal Abelian gauge [32] to rotate the color vector of the links as much as possible in, say, the σ_3-direction by maximizing

$$R = \sum_{x,\mu} \mathrm{tr}[U_\mu(x)\sigma_3 U_\mu^\dagger(x)\sigma_3]\,. \tag{2}$$

Afterwards, the link variables are replaced by their diagonal part

$$U_\mu(x) = a_0\mathbb{1} + i\vec{a}\cdot\vec{\sigma} \to u_\mu(x) = \frac{1}{\sqrt{a_0^2+a_3^2}}[a_0\mathbb{1} + ia_3\sigma_3] = \begin{pmatrix} \exp\{i\theta_\mu(x)\} & 0 \\ 0 & \exp\{-i\theta_\mu(x)\} \end{pmatrix}. \tag{3}$$

Consider a 3-dimensional cube on the lattice. Normally, the total magnetic flux out of the cube vanishes due to $\mathrm{div}\,\vec{B} = 0$. If the cube contains a monopole, there would be a nonzero net flux of the (unphysical) Dirac string, which compensates the physical monopole flux. The magnetic charge inside the cube is defined by [33]

$$m = \frac{1}{2\pi}\sum_p \bar{\theta}_p\,. \tag{4}$$

θ_p is the sum of the angles θ_μ around one plaquette p; $\sum_p \theta_p$ is always zero as a consequence of the Bianchi identity. $\bar{\theta}_p$ is $\theta_p + 2\pi k$ with k such that $\bar{\theta}_p$ falls into the range $[-\pi,\pi]$. If the absolute value of all plaquette angles is smaller than π, $\bar{\theta}_p = \theta_p$ and $m = 0$, as usual. Plaquettes which are greater than π are pierced by the Dirac string, at the end of which a monopole is located. $\bar{\theta}_p$ discards the flux caused by the Dirac string and a value $m \neq 0$ results.

Now let us return to center vortices. Traversing a thick vortex sheet, the link variables change gradually, building up to a center element. Pictured in group space of $SU(2) \simeq S^3$, we travel along a path from unity to the antipode $-\mathbb{1}$. After Abelian projection, only one possible direction for the path remains and this path will go either in $+\sigma_3$ or in $-\sigma_3$ direction. We can use this sign to allocate an orientation to every patch of the vortex surface. The sign also corresponds to the direction of the center flux bundled within the vortex, which is quantized in units $\pm\pi$. Where regions of opposite orientation touch, the flux jumps by 2π, indicating the presence of a sink or source, *i.e.*, a magnetic monopole carrying a quantized magnetic charge. To summarize, a center vortex can be imagined as a chain of magnetic monopoles, whose flux is bundled within the vortex surface. The monopole worldlines divide the vortex sheet into patches of different orientations.

A. Plane vortices

In $SU(2)$ lattice gauge theory, plane vortices parallel to two of the coordinate axes are defined by links varying in a $U(1)$ subgroup of $SU(2)$. This $U(1)$ subgroup is generated by one of the Pauli matrices σ_i, *i.e.*, $U_\mu = \exp(\mathrm{i}\phi\sigma_i)$. The direction of the flux and the orientation of the vortices are determined by the gradient of the angle ϕ, which we choose as a piecewise linear function of the coordinate perpendicular to the vortex. The explicit functions for ϕ are given in Eq. (2.1) of [34]. Upon traversing a vortex sheet, the angle ϕ increases or decreases by π within a finite thickness of the vortex. Center projection leads to a (thin) P-vortex at half the thickness [18]. If we consider these thick, planar vortices intersecting orthogonally, see Fig. 1a, each intersection carries a topological charge with modulus $|Q| = 1/2$, whose sign depends on the relative orientation of the vortex fluxes [35].

B. The Colorful Spherical Vortex

The nonorientable spherical vortex of radius R and thickness Δ was introduced in [26] and analyzed in more detail in [27] and [29]. It is constructed with the following $SU(2)$ links:

$$U_\mu(x^\nu) = \begin{cases} \exp\left(\mathrm{i}\alpha(|\vec{r}-\vec{r}_0|)\vec{n}\cdot\vec{\sigma}\right) & t = t_i, \mu = 4 \\ \mathbb{1} & \text{elsewhere} \end{cases} \quad \text{with} \quad \vec{n}(\vec{r},t) = \frac{\vec{r}-\vec{r}_0}{|\vec{r}-\vec{r}_0|}\,, \tag{5}$$

where $\vec{r}$ is the spatial part of x_ν and the profile function α is either one of α_+, α_-, which are defined by

$$\alpha_+(r) = \begin{cases} 0 \\ \frac{\pi}{2}\left(1 - \frac{r-R}{\frac{\Delta}{2}}\right) \\ \pi \end{cases} \quad \dots \quad \alpha_-(r) = \begin{cases} \pi & r < R - \frac{\Delta}{2} \\ \frac{\pi}{2}\left(1 + \frac{r-R}{\frac{\Delta}{2}}\right) & R - \frac{\Delta}{2} < r < R + \frac{\Delta}{2} \\ 0 & R + \frac{\Delta}{2} < r \end{cases}. \tag{6}$$

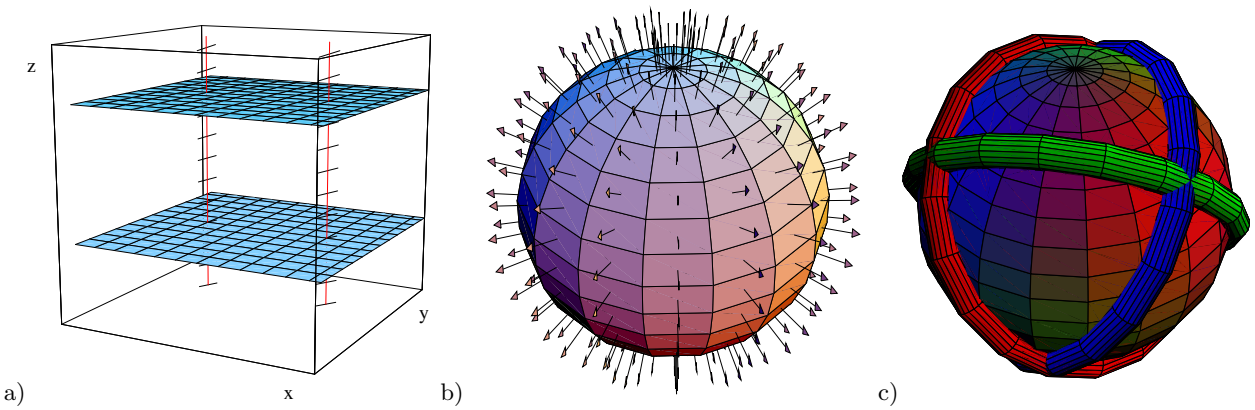

FIG. 1. a) Two plane vortex pairs intersecting in four space-time points. b) The color structure of the vortex surface from the hedgehog configuration leads to c) monopole lines after Abelian projection in the maximal Abelian gauge.

This means that all links are equal to $\mathbb{1}$ except for the t-links in a single time slice at fixed $t = t_i$. The phase changes from 0 to π from inside to outside for $\alpha_+(r)$ (or vice versa for $\alpha_-(r)$). The graph of $\alpha_-(r)$ is plotted in Fig. 2 in [26], giving a hedgehog-like configuration, since the color vector $\vec{n}$ points in the "radial" direction $\vec{r}/r$ at the vortex radius R, see Fig. 1b. The check that this configuration is a vortex is done with maximal center gauge fixing and center projection and results in a P-vortex forming a lattice representation of a 3-sphere of radius R at time slice t_i. The color structure of the thick vortex leads to a monopole loop on a great circle of the P-vortex after fixing to maximal Abelian gauge and Abelian projection. The direction of the loop depends on the $U(1)$ subgroup chosen as Abelian degrees of freedom. For the subgroup defined by the Pauli matrices σ_1, σ_2 or σ_3 the monopole loops are in the yz-, zx- and xy-plane, respectively. This is indicated schematically in Fig. 1c with three colors.

The hedgehog-like structure is crucial for our analysis. The t-links of the spherical vortices fix the holonomy of the time-like loops, defining a map $U_t(\vec{x}, t = t_i)$ from the xyz-hyperplane at $t = t_i$ to $SU(2)$. Because of the periodic boundary conditions, the time slice has the topology of a 3-torus. But, actually, we can identify all points in the exterior of the 3 dimensional sphere since the links there are trivial. Thus the topology of the time slice is $\mathbb{R}^3 \cup \{\infty\}$ which is homeomorphic to S^3. A map $S^3 \to SU(2)$ is characterized by a winding number

$$N = -\frac{1}{24\pi^2} \int d^3x \, \epsilon_{ijk} \, \mathrm{Tr}[(U^\dagger \partial_i U)(U^\dagger \partial_j U)(U^\dagger \partial_k U)],$$

resulting in $N = -1$ for positive and $N = +1$ for negative spherical vortices. Obviously such windings, given by the holonomy of the time-like loops of the spherical vortex, influence the Atiyah-Singer index theorem [5–8, 36, 37], giving a topological charge $Q = -1$ for positive and $Q = +1$ for negative spherical vortices (antivortices). Hence, spherical vortices attract Dirac zero modes similar to instantons. In [29] we showed that the spherical vortex is in fact a vacuum-to-vacuum transition in the time direction which can even be regularized (smoothed out in the time direction) to give the correct topological charge also from gluonic definitions (see also [38] for more details).

III. DIRAC EIGENMODES

According to the Banks-Casher analysis [39], chiral symmetry breaking (χSB) is necessarily associated with a finite density of near-zero eigenmodes of the chiral-invariant Dirac operator, resulting in a finite chiral condensate, the order parameter of chiral symmetry breaking. We compute the lowest-lying chiral eigenvectors $\chi_{R,L}$ and eigenvalues $|\lambda| \in [0, 1]$ of the overlap Dirac operator

$$D_{ov} = \frac{1}{2}\left[1 + \frac{D_W}{\sqrt{D_W^\dagger D_W}}\right] \tag{7}$$

with the kernel Wilson Dirac operator D_W [40]. Henceforth we will simply write λ instead of $|\lambda|$ and assume it to be the absolute value of the two complex conjugate eigenvalues of D_{ov} if $\lambda \neq 0, 1$. We will however distinguish between right- and left-handed zero modes of D_{ov}. When speaking of an eigenmode, we always mean both of the eigenvectors $\psi_\pm$ belonging to one value of $\lambda \neq 0$, which have the same scalar and chiral densities. For convenience,

we will number the eigenfunctions in ascending order of the eigenvalues. #0+ denotes the right-handed zero mode, #0– the left-handed zero mode. #1 labels the lowest nonzero mode, #2 the second lowest etc. Their eigenvalues are referred to as λ#0+, λ#0–, λ#1, etc., and their densities as ρ#0+, etc. Finally, we will name near-zero modes which emerge from would-be zero modes also by #0 for good reasons, which will be discussed later.

The corresponding eigenvectors are given by

$$\psi_\pm = \frac{1}{\sqrt{2}}(\chi_R \pm i\chi_L). \tag{8}$$

They have scalar and chiral densities

$$\rho = \psi_\pm^\dagger \psi_\pm = \frac{1}{2}(\chi_R^\dagger \chi_R + \chi_L^\dagger \chi_L)\,, \tag{9}$$

$$\rho_+ = \psi_\pm^\dagger \frac{1}{2}(1+\gamma_5)\psi_\pm = \frac{1}{2}(\chi_R^\dagger \chi_R)\,, \tag{10}$$

$$\rho_- = \psi_\pm^\dagger \frac{1}{2}(1-\gamma_5)\psi_\pm = \frac{1}{2}(\chi_L^\dagger \chi_L)\,, \tag{11}$$

$$\rho_5 = \psi_\pm^\dagger \gamma_5 \psi_\pm = \frac{1}{2}(\chi_R^\dagger \chi_R - \chi_L^\dagger \chi_L) = \rho_+ - \rho_-\,. \tag{12}$$

The chiral density ρ_5 is important to assess the local chirality properties, in particular to test the notion that the near-zero modes arise from the splitting of exact zero modes localized at lumps of topological charge.

In a gauge field with topological charge $Q \neq 0$, D_{ov} has $|Q|$ exact zero modes with chirality $-\mathrm{sign}Q$, and an equal number of eigenvectors of opposite chirality and eigenvalue 1 (doubler modes). This is required in order that $\mathrm{Tr}\gamma_5 = 0$. The topological charge is

$$Q = \mathrm{Tr}(\gamma_5 D_{ov}) = n_- - n_+ = \mathrm{ind}D_{ov}\,, \tag{13}$$

as for any Ginsparg-Wilson operator.

The plot titles of the density plots (see *e.g.* Fig. 2) give the x- and y-coordinates of the shown zt-slice, the chirality (*i.e.*, "chi=0" means we plot ρ_5, "chi=1" would be ρ_+ and "chi=-1" ρ_-), the numbers of plotted modes ("n=1-1" means we plot ρ#1, "n=1-2" would be ρ#1 + ρ#2) and the maximal density in the plotted area ("max=..." - some maxima are cut off in order to resolve other substructures). For instanton and spherical vortex configurations we use $12^3 \times 24$-lattices and always plot xt-slices at $y = z = 6$ since they are symmetric in spatial directions around their centers at $x = y = z = 6.5$. For plane vortex configurations we use 16^4-lattices; the plotted slices vary.

A. Eigenvalue Spectrum of the free Dirac operator

In this section we will analytically calculate the eigenvalues of the massless free Dirac operator. These eigenvalues and their multiplicity will come handy later when we compare the eigenvalues for different gauge field configurations to the eigenvalues for the free case. The free continuum Dirac operator for massless fermions is given by $D = \gamma_\mu \partial_\mu$, where γ_μ are the Euclidean Dirac matrices. We want to solve the Dirac equation $D_{\alpha\beta}\ \psi_\beta(x) = \lambda\ \psi_\alpha(x)$. Using the well know ansatz of plane wave functions $\psi_\alpha(x) = u_\alpha\ \exp(ip_\mu x_\mu)$, one gets the eigenvalues of the free continuum operator $\lambda = \pm i\sqrt{p_\mu p_\mu}$. Identifying the eigenvalue λ with the fermion mass M makes clear, that this is simply the relativistic energy momentum relation in Euclidean space given by $M^2 = E^2 + p^2$, where we have denoted p_4^2 by E^2 and $p_i p_i$ by p^2. Note that both the eigenvalue for the plus and the minus sign have a degeneracy of two, which gives in total four eigenvalues for the 4×4 Dirac matrix (4×4 Dirac indices). Additional degeneracy comes from the color indices. The free Dirac operator is color blind. Therefore, the degeneracy of the different eigenvalues is multiplied by n_{col}, where n_{col} is the range of the color indices. For the overlap Dirac operator the eigenvalues can also be calculated analytically for the free case using the lattice ansatz $\psi_\alpha(n) = u_\alpha\ \exp(i\ a\ p_\mu n_\mu)$, with the lattice sites n_μ and yield the continuum solutions with corrections of orders of a^2:

$$D_{ov}(p_\mu) = \frac{1}{2}\left[1 + \frac{i\gamma_\mu \sin(p_\mu) - M(p_\mu)}{\sqrt{\sum_\mu \sin(p_\mu)^2 + M^2(p_\mu)}}\right] \tag{14}$$

with $M(p_\mu) = M - \sum_\mu (1 - \cos(p_\mu))$. Here $a = 1$ and $M = 1$ in the free case. This gives ($H_{ov} = \gamma_5 D_{ov}$):

$$H_{ov}^2(p_\mu) = D_{ov}^\dagger D_{ov} = \frac{1}{2}\left[1 - \frac{M(p_\mu)}{\sqrt{\sum_\mu \sin(p_\mu)^2 + M^2(p_\mu)}}\right] = \lambda^2 \tag{15}$$

with expected multiplicities ($H^2_{ov}(p_\mu)$ is a diagonal 4×4 matrix). For $p_\mu << 1$ we get

$$\lambda^2 = \frac{p_\mu p_\mu}{4M^2}(1 + O(p_\mu p_\mu)) \,. \tag{16}$$

With the normalization of Eq. (7), which leads to $\lambda^2 \in [0, 1]$, a wave function renormalization is needed to convert to the usual continuum normalization. This compensates the factor $\frac{1}{4M^2}$, see e.g. Eq. (6) in [41], giving the usual free Dirac eigenvalues in the continuum limit. Note that the plane wave ansatz is periodic, not only in x_μ or lattice indices n_μ, but also in p_μ. This means, that p_μ and $p_\mu + \frac{2\pi z_\mu}{a}$ (with $z_\mu \in \mathbb{Z}$) correspond to the same eigenfunction. Therefore, in order to get the correct multiplicities for the eigenvalues, we have to restrict the range of p_μ to

$$-\frac{\pi}{a} < p_\mu \leq \frac{\pi}{a} \,. \tag{17}$$

For the usual periodic boundary conditions in spatial directions and periodic or antiperiodic boundary conditions in temporal direction, the allowed values for p_μ are

$$p_i = \frac{2n\pi}{aN_{sp}}, \qquad p_4 = \begin{cases} \frac{2n\pi}{aN_t} & \text{for periodic BC} \\ \frac{(2n+1)\pi}{aN_t} & \text{for antiperiodic BC} \end{cases}, \qquad n \in \mathbb{Z} \,,$$

where N_{sp} is the spatial and N_t the temporal extent of the lattice. The total multiplicity of an eigenvalue λ is given by

$$n_{mult}(\lambda) = 2 \; n_{col} \; n_p(\lambda),$$

where $n_p(\lambda)$ is the number of different p_μ corresponding to a particular λ. The factor two comes from the Dirac indices as discussed above. Let us now have a quick look at the multiplicity of the eigenvalues for one particular lattice size, *i.e.*, $N_{sp} = 12$ and $N_t = 24$, which we will use later for our lattice configurations. We assume antiperiodic boundary conditions in temporal direction, $a = 1$ and a $SU(2)$ gauge field theory (*i.e.*, $n_{col} = 2$). The momentum vectors corresponding to the lowest eigenvalues are then given by $p_i = 0$ and $p_4 = \pm\pi/24$. Therefore, we have $n_p(\lambda\#1) = 2$ for the lowest eigenvalues $\lambda\#1$. That means, we get a multiplicity $n_{mult}(\lambda\#1) = 2 \; n_{col} \; n_p(\lambda\#1) = 8$. For the second lowest eigenvalues $\lambda\#2$ we have $p_i = 0$ and $p_4 = \pm 3\pi/24 = \pm\pi/8$ and therefore another degeneracy of eight. Then we get $p_i = \pm\pi/6$ (with $i \in \{1, 2, 3\}$) and $p_4 = \pm\pi/24$, *i.e.*, $n_p(\lambda\#3) = 12$. This gives a multiplicity $n_{mult}(\lambda\#3) = 48$.

Fig. 2 shows the chiral density of free overlap eigenmodes obtained numerically using the MILC code. The modes are found with the Ritz functional algorithm [42, 43] with random start and for degenerate eigenvalues the eigenmodes span a randomly oriented basis in the degenerate subspace. Therefore the numerical modes presented in Fig. 2 are linear combinations of plane waves with $\pm p_\mu$ and show plane wave oscillations of $2p_\mu$ in the chiral density. The first eight degenerate modes consist of plane waves with $p_4 = \pm\pi/24$, hence there is one sine (cosine) oscillation in time direction, the next eight have $p_4 = \pm 3\pi/24$, *i.e.*, three oscillations in the time direction. The oscillations of χ_R and χ_L are separated by half an oscillation length, *i.e.*, the maxima of ρ_+ correspond to minima of ρ_- and vice versa. Accordingly, the scalar density $\rho(x_\mu) = \frac{1}{2}(\chi^\dagger_R(x_\mu)\chi_R(x_\mu) + \chi^\dagger_L(x_\mu)\chi_L(x_\mu)) = 1/N_V$ is constant ($N_V \ldots$ lattice volume).

B. Zero Modes and Instantons

An instanton field gives rise to an exact zero mode (the precise expression is given in *e.g.* [44]). Its probability density

$$\rho(x) = \frac{2}{\pi^2} \frac{R^2}{(x - x_0)^2 + R^2} \tag{18}$$

is localized at the instanton core x_0, with a half-radius of the instanton parameter R. Since the zero mode is exactly chiral, its chiral density $\psi^\dagger\gamma_5\psi$ equals $\pm\rho$.

In the instanton liquid model the near-zero modes originate from the overlap of the would-be zero modes carried by individual instantons and anti-instantons. If the overlap is not too large, one expects that the resulting near-zero modes still exhibit definite chirality *locally*. This picture predicts characteristic properties of the low-lying modes [45]:

- Their probability density should be clearly peaked, indicating the location of instantons.

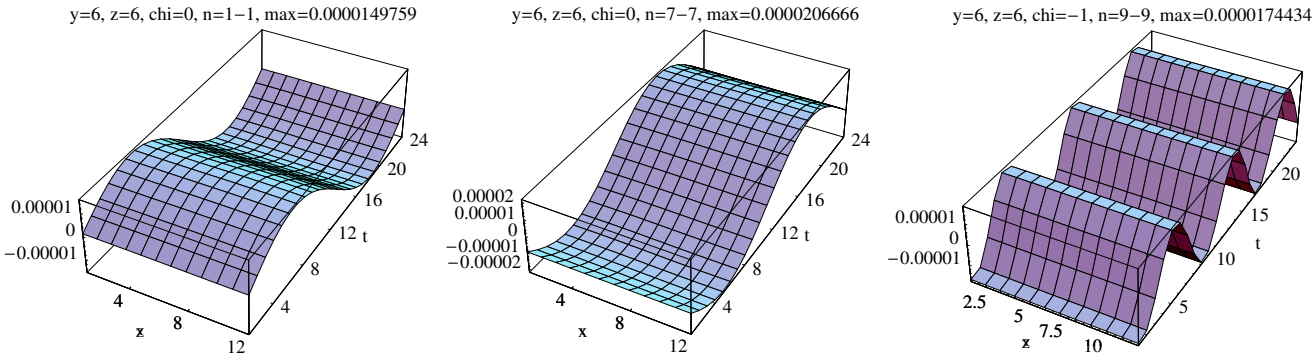

FIG. 2. Chiral density of the low-lying eigenmodes of the free overlap Dirac operator: $\rho_5\#1$ (left), $\rho_5\#7$ (center) $\rho_5\#9$ (right). The modes clearly show the plane wave behavior with oscillations of $2p_\mu$ (see text).

- The local chirality at the peaks should match the sign of the topological charge and the size of the chiral lump should be correlated to the extension of the topological structure.
- As an instanton and an anti-instanton approach each other, the eigenvalues should be shifted further away from zero and the localization and local chirality properties should fade.

Numerical evidence supporting these assumptions about the local chirality structure of the low-lying Dirac modes are presented in *e.g.* [46] and [47]. Here we want to analyze these issues for center vortices.

C. Zero Modes and Center Vortices

Reinhardt et al. [48] analytically calculate the exact zero modes of the Dirac operator in the background of plane vortices, both nonintersecting and perpendicularly intersecting ones, for an Abelian $U(1)$ gauge field on $\mathbb{R}^2, \mathbb{R}^4, \mathbb{T}^2$ and $\mathbb{T}^4$.

The first vortex field of interest consists of two (anti)parallel fluxes on a two-torus. Because of a two-dimensional translation symmetry we can identify this with the four-dimensional configuration of a single vortex pair presented in Sec. II A. The second example contains four flat vortices on a four-torus, which intersect orthogonally in four points. This corresponds to the configuration shown in Fig. 1a.

We want to discuss the boundary conditions used in [48]. The four-dimensional problem can be reduced to two two-dimensional ones because of the translation invariance parallel to the vortex sheets. It therefore suffices to deal with the $\mathbb{T}^2$ case. The boundary conditions for a gauge field on $\mathbb{T}^2$ are specified by the two transition functions Ω_x, Ω_y. In a suitable gauge, it is possible to set $\Omega_x = 1$. The co-cycle condition then turns into a periodicity condition

$$\Omega_y(x + L_x) = \Omega_y(x) \tag{19}$$

for $\Omega_y(x)$, which lives only at the boundary of the rectangle which represents the torus. Therefore Ω_y defines a function $S^1 \to S^1$ belonging to a class of the homotopy group $\pi_1(S^1) \simeq \mathbb{Z}$. Its winding number n determines the magnetic flux through the xy-plane by

$$\Phi := \oint A_\mu \mathrm{d}x_\mu = 2\pi n\,. \tag{20}$$

To prove this, we simply perform the line integral over the boundary of the rectangle resulting from cutting up the torus. We set $\Omega_y(x) = \exp\{i\chi(x)\}$. Since Ω_y is periodic, $\chi(x + L_x) = \chi(x) + 2\pi n$. Then

$$\begin{aligned}
\Phi &= \int_0^{L_x} A_x(x,0)\mathrm{d}x + \int_0^{L_y} A_y(L_x,y)\mathrm{d}y - \int_0^{L_x} A_x(x,L_y)\mathrm{d}x - \int_0^{L_y} A_y(0,y)\mathrm{d}y \\
&= \int_0^{L_x} A_x(x,0)\mathrm{d}x + \int_0^{L_y} A_y(0,y)\mathrm{d}y - \int_0^{L_x} [A_x(x,0) - \partial_x\chi(x)]\mathrm{d}x - \int_0^{L_y} A_y(0,y)\mathrm{d}y \\
&= \int_0^{L_x} \partial_x\chi(x)\mathrm{d}x = \chi(L_x) - \chi(0) = 2\pi n\,.
\end{aligned} \tag{21}$$

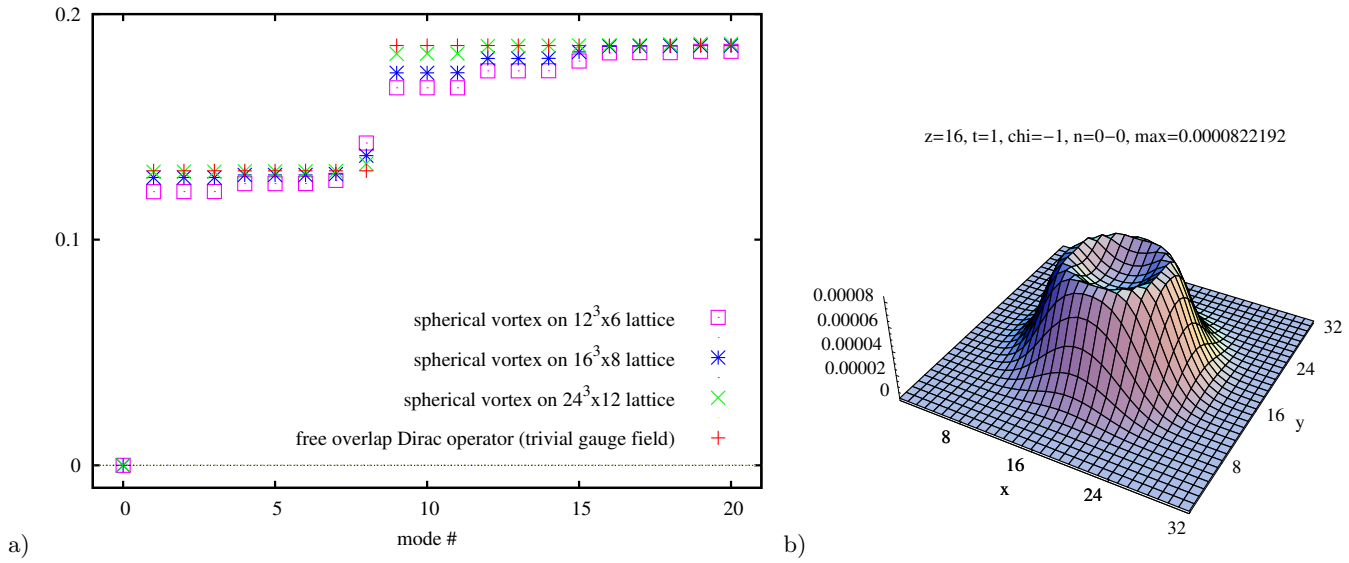

FIG. 3. a) The lowest eigenvalues for the spherical vortex with $R = d = 3a$ compared to the eigenvalues of the free Dirac operator (red crosses). Eigenvalues are calculated on a $12^3 \times 6$ lattice with relative lattice constant $a = 2$ (magenta boxes), on a $16^3 \times 8$ lattice with $a = \frac{3}{2}$ (blue stars) and on a $24^3 \times 12$ lattice with $a = 1$ (green crosses). The multiplicity of $\lambda\#1$ is eight, of $\lambda\#2$ 48. b) Spatial distribution of the zero mode, mainly located at the vortex core.

Consequently, the flux on $\mathbb{T}^2$ is quantized. Note that this would not hold for SU(2) since $\pi_1(S^3) = 1$. To create two vortices which carry a flux of $+\pi$ each, Reinhardt et al. use $\Omega_y = \exp\{2\pi i x\}$. Returning finally to the fermion field, it obeys boundary conditions consistent with gauge invariance,

$$\psi(x, y + L_y) = \Omega_y(x)\psi(x, y)\,. \tag{22}$$

In [34] we analyzed the zero modes for plane vortex configurations and found good agreement with the results obtained by Reinhardt *et al.* [48]. The discrepancies discussed in our work originate in the finite thickness of our vortex configurations because of finite lattice sizes.

We conclude this section with a quick discussion of the eigenvalues for the spherical vortex. As already mentioned, there always occurs exactly one zero mode, a positive chirality one for the spherical vortex and a negative chirality zero mode for the antivortex. The lowest nonzero modes can be seen as some sort of modified eigenmodes of the free Dirac operator. This point of view is motivated by the results presented in Fig. 3a. In this diagram, one can see the eigenvalues for configurations with vortices of the same size in lattice units but different spatial N_{sp} and temporal N_t lattice extents. In other words, the vortex gets smaller while the lattice gets finer. One sees from the figures, that the nonzero eigenvalues converge to eigenvalues of the free Dirac operator as the vortex gets smaller and smaller. For the investigated eigenvalues, there seems to be a one to one correspondence between the eigenvalues of the free Dirac operator and the nonzero eigenvalues of the Dirac operator for the vortex configuration. The zero mode is not a lowered nonzero mode, it occurs in addition to the low lying modes. Because the total number of eigenmodes only depends on the lattice size, the number of complex eigenvalues is lowered by two (because of the zero and the doubler mode) for the vortex configuration in comparison to the free case. Note that we still can have a one to one correspondence between all the complex eigenvalues for the vortex and the free case. One can see this by remembering that the correspondence is established in the limit of an infinitely large lattice.

IV. INTERACTIONS BETWEEN TOPOLOGICAL OBJECTS

We want to discuss the Dirac equation for a gauge field $\mathcal{A}_\mu = \mathcal{A}_{1\mu} + \mathcal{A}_{2\mu}$ consisting of two fields $\mathcal{A}_{1\mu}$ and $\mathcal{A}_{2\mu}$ which are separated in Euclidean space and have nonvanishing topological charge Q_i. Therefore, the Dirac operators D_1 for $\mathcal{A}_{1\mu}$ alone and D_2 for $\mathcal{A}_{2\mu}$ alone would have at least one zero mode. In the following, the zero modes of D_1 and D_2 will be called would-be zero modes. Lets discuss the case in which $\mathcal{A}_{1\mu}$ has $Q_1 = 1$ and $\mathcal{A}_{2\mu}$ has $Q_2 = -1$. For simplicity we assume that D_1 has only one left handed zero mode $|\,\psi_1\rangle$ and D_2 only one right handed zero mode $|\,\psi_2\rangle$. Clearly, this two would-be zero modes are orthogonal, they can be part of an orthogonal basis. Let us now have

a look at the Dirac operator in this orthogonal basis. In particular we are interested in the upper left 2×2 block

$$\begin{pmatrix} \langle \psi_1 \mid D \mid \psi_1 \rangle & \langle \psi_1 \mid D \mid \psi_2 \rangle \\ \langle \psi_2 \mid D \mid \psi_1 \rangle & \langle \psi_2 \mid D \mid \psi_2 \rangle \end{pmatrix} \tag{23}$$

of the Dirac matrix. The continuum Dirac operator D is given by

$$\begin{aligned} D &= \gamma_\mu \ (\partial_\mu + \mathrm{i}\mathcal{A}_\mu(x)) = \gamma_\mu \ (\partial_\mu + \mathrm{i}\mathcal{A}_{1\mu}(x) + \mathrm{i}\mathcal{A}_{2\mu}(x)) \\ &= D_1 + \gamma_\mu \mathrm{i}\mathcal{A}_{2\mu}(x) = D_2 + \gamma_\mu \ \mathrm{i}\mathcal{A}_{1\mu}(x)\,. \end{aligned} \tag{24}$$

The first element of (23) therefore evaluates to

$$\langle \psi_1 \mid D \mid \psi_1 \rangle = \langle \psi_1 \mid D_1 \mid \psi_1 \rangle + \langle \psi_1 \mid \gamma_\mu \ \mathrm{i}\mathcal{A}_{2\mu}(x) \mid \psi_1 \rangle = 0\,. \tag{25}$$

One can see that $\langle \psi_1 \mid \gamma_\mu \ \mathrm{i}\mathcal{A}_{2\mu}(x) \mid \psi_1 \rangle$ vanishes from

$$\begin{aligned} \langle \psi_1 \mid \gamma_\mu \ \mathrm{i}\mathcal{A}_{2\mu}(x) \mid \psi_1 \rangle &= \langle \psi_1 \mid \gamma_\mu \ \mathrm{i}\mathcal{A}_{2\mu}(x) \ {\gamma_5}^2 \mid \psi_1 \rangle \\ &= - \ \langle \psi_1 \mid \gamma_5 \ \gamma_\mu \ \mathrm{i}\mathcal{A}_{2\mu}(x) \ \gamma_5 \mid \psi_1 \rangle = - \ \langle \psi_1 \mid \gamma_\mu \ \mathrm{i}\mathcal{A}_{2\mu}(x) \mid \psi_1 \rangle \ ,. \end{aligned} \tag{26}$$

In the same way one can prove

$$\langle \psi_2 \mid D \mid \psi_2 \rangle = 0\,. \tag{27}$$

Let us now calculate the off-diagonal terms. The first off-diagonal term evaluates to

$$\langle \psi_1 \mid D \mid \psi_2 \rangle = \langle \psi_1 \mid D_2 \mid \psi_2 \rangle + \langle \psi_1 \mid \gamma_\mu \ \mathrm{i}\mathcal{A}_{1\mu}(x) \mid \psi_2 \rangle = 0 + c = c\,. \tag{28}$$

Here c stands for the overlap integral $\langle \psi_1 \mid \gamma_\mu \ \mathrm{i}\mathcal{A}_{1\mu}(x) \mid \psi_2 \rangle$. In general, c will be large for eigenmodes that overlap a lot, and small for eigenmodes that overlap only a little. Note that it is crucial that $\mid \psi_1 \rangle$ and $\mid \psi_2 \rangle$ have different chirality. Otherwise, by the same argument as used in (26), the overlap integral would have to vanish. The second off-diagonal term of the upper-left 2×2 block is

$$\langle \psi_2 \mid D \mid \psi_1 \rangle = \left(\langle \psi_1 \mid D^\dagger \mid \psi_2 \rangle \right)^* = (- \ \langle \psi_1 \mid D \mid \psi_2 \rangle)^* = -c^*\,. \tag{29}$$

Here it was used that the continuum Dirac Operator D is antihermitian, *i.e.*, $D^\dagger = -D$.

Combining (25), (27), (28) and (29), the upper left 2×2 block of the Dirac matrix reads

$$\begin{pmatrix} 0 & c \\ -c^* & 0 \end{pmatrix}. \tag{30}$$

This 2×2 block can easily be diagonalized. The eigenvalues $\lambda_{1,2}$ and the normalized eigenvectors $\psi'_{1,2}$ of (30) are

$$\lambda_{1,2} = \pm \mathrm{i}\sqrt{cc^*} = \pm \mathrm{i}|c|, \quad \psi'_{1,2} = \frac{1}{\sqrt{2}} \begin{pmatrix} \pm \mathrm{i}\sqrt{\frac{c}{c^*}} \\ 1 \end{pmatrix}. \tag{31}$$

This means that the interaction transforms the two (would-be) zero modes into two near-zero modes. Those near-zero modes also occur additionally to the free Dirac eigenmodes and therefore we still enumerate them like zero modes by #0. The strength of the interaction quantified by the overlap integral c determines the size of the near-zero eigenvalue. Note that the new near-zero modes consist in equal parts of the would-be zero modes $\mid \psi_1 \rangle$ and $\mid \psi_2 \rangle$. Therefore the scalar and chiral densities of the near-zero modes are simply an average of the densities of the would-be zero modes.

So far we have ignored everything except the upper left 2×2 block of the Dirac matrix. To get exact eigenmodes we clearly have to diagonalize the whole Dirac matrix and not only this 2×2 block. However, (31) represents a legitimate approximation to the exact eigenvalues and eigenmodes if the elements of the form

$$\langle \psi_j \mid D \mid \psi_{1,2} \rangle = \langle \psi_j \mid \gamma_\mu \ \mathrm{i}\mathcal{A}_{2,1\mu}(x) \mid \psi_{1,2} \rangle \quad \text{with} \quad j > 2$$

are a lot smaller than the overlap integral $c = \langle \psi_1 \mid \gamma_\mu \ \mathrm{i}\mathcal{A}_{1\mu}(x) \mid \psi_2 \rangle$. Usually this will be the case, because $\mid \psi_1 \rangle$ is localized at $\mathcal{A}_{1\mu}$ and $\mid \psi_j \rangle$ with $j > 2$ is not. Let us also have a quick look at what happens when we have two would-be zero modes with the same chirality. In this case also the off-diagonal terms of the upper left 2×2 matrix vanish and the would-be zero modes are actual zero modes.

Note that the mechanism discussed in this section is the basis for the instanton liquid model of spontaneous chiral symmetry breaking (see [44] for a detailed review). In the instanton liquid model the QCD-vacuum consist of an ensemble of instantons and anti-instantons whose would-be zero modes split into near-zero modes because of interactions. Therefore, one gets a nonvanishing eigenmode density around zero, which gives via the Banks-Casher relation a finite chiral condensate and broken chiral symmetry. Clearly, one can construct such a model also with other topological objects, as will be shown in the next section for center vortices.

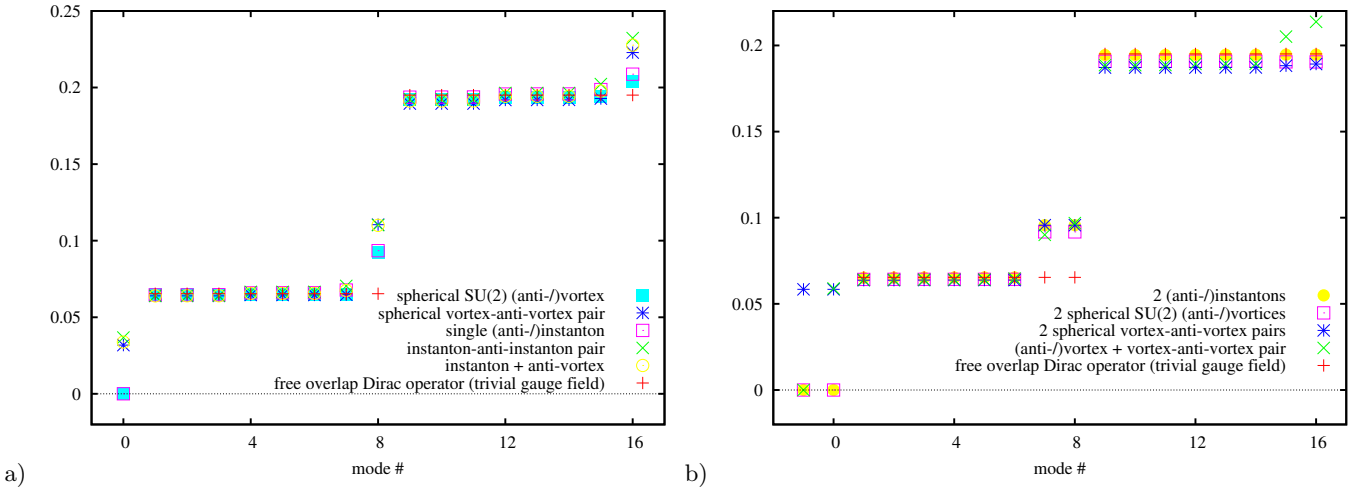

FIG. 4. The lowest overlap eigenvalues for instanton and spherical vortex configurations compared to the eigenvalues of the free (overlap) Dirac operator.

V. VORTICES AND χSB

In Sec. II we discussed the various possibilities of vortices to create topological charge, *i.e.*, via writhing and intersection points as well as through their color structure. In previous works we presented results on the attraction of zero modes for flat [34] and spherical [26–29]vortex configurations. Here we present some results on how vortices form near-zero modes from would-be zero modes through interactions.

A. Spherical Vortices and Instantons

We start with spherical vortices and show that their effects on fermions is pretty much the same as those of instantons. We have shown in Fig. 3 that they attract a zero mode and its scalar density peaks at the vortex surface. We interpreted the nonzero modes as eigenmodes of the free Dirac operator, which are shifted slightly because of their interaction with the nontrivial gauge field content. In Fig. 4a we see that a single instanton has nearly exactly the same eigenvalues as a single spherical vortex. In Fig. 5 we show that even the chiral densities of the lowest eigenmodes distribute similarly, except for the fact that the response of the fermions to the spherical vortex is squeezed in the time direction, since the vortex is localized in a single time slice ($t = 5$). Another interesting issue is that the nonzero eigenmodes show nice plane wave oscillations, like the free eigenmodes in Fig. 2, mode #8 however shows some similarity to the zero mode, its eigenvalue is also clearly enhanced compared to the free spectrum. This is only a side remark however, as we are not sure how to interpret this and it does not seem to be important for the creation of near-zero modes since we observe the same effect for instantons.

We further plot the spectra of instanton–anti-instanton, spherical vortex-antivortex and instanton-antivortex pairs in Fig. 4a. We again see nearly exactly the same eigenvalues for instanton or spherical vortex pairs, but now we get instead of two would-be zero modes a near-zero mode for each pair. The chiral density plots in Fig. 6 for the instanton–anti-instanton pair and Fig. 7 for the spherical vortex-antivortex pair show, besides the similar densities, that the near-zero mode is a result of two chiral parts corresponding to the two constituents of the pairs. The nonzero modes can again be identified with the free overlap modes with the same side remark for mode #8.

Finally in Fig. 4b we plot the eigenvalues of two (anti-)instantons and two spherical (anti)vortices giving topological charge $Q = 2$ ($Q = -2$) and therefore two zero modes, two vortex-antivortex pairs with two near-zero modes and a configuration with two vortices and an antivortex (*i.e.*, a single vortex plus one vortex-antivortex pair) giving one zero mode ($Q = 1$) and one near-zero mode. The chiral densities for the last configuration in Fig. 8 show that the zero mode peaks at both spherical vortices, the near-zero mode again consists of two chiral parts from the (second/would-be) zero mode of the two vortices and the (would-be) zero mode of the antivortex. Now the modes #7 and #8 clearly deviate from the free eigenvalues showing similar densities as the zero and the near-zero mode respectively. The results clearly show that we may draw the same conclusions for spherical vortices as for instantons concerning the creation of near-zero modes.

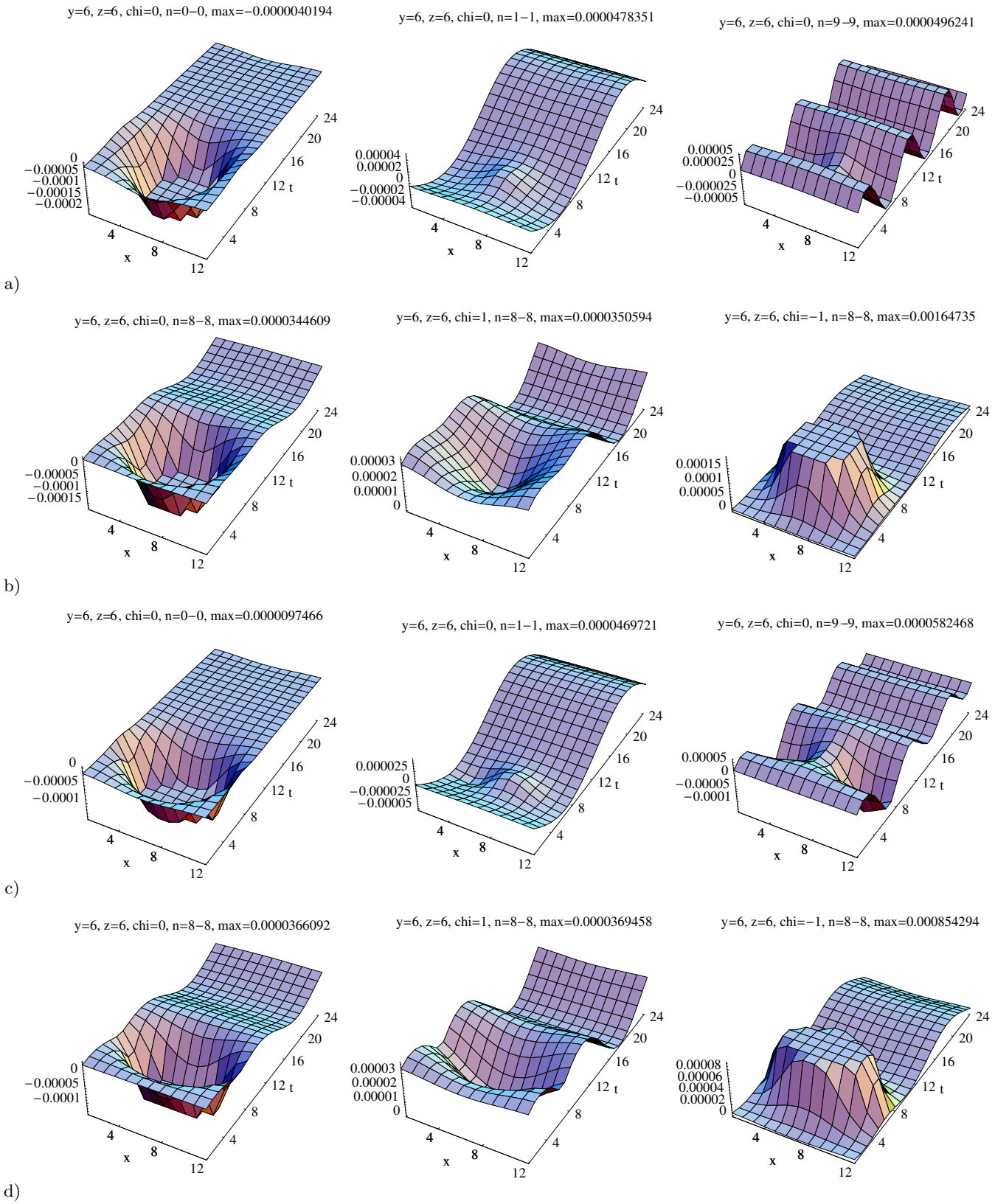

FIG. 5. Chiral densities of overlap eigenmodes: a) zero mode (left), first (center), ninth (right) and b) eighth (ρ_5 left, ρ_+ center and ρ_- right) nonzero modes for an instanton; c) and d) the same as a) and b) but for a spherical vortex.

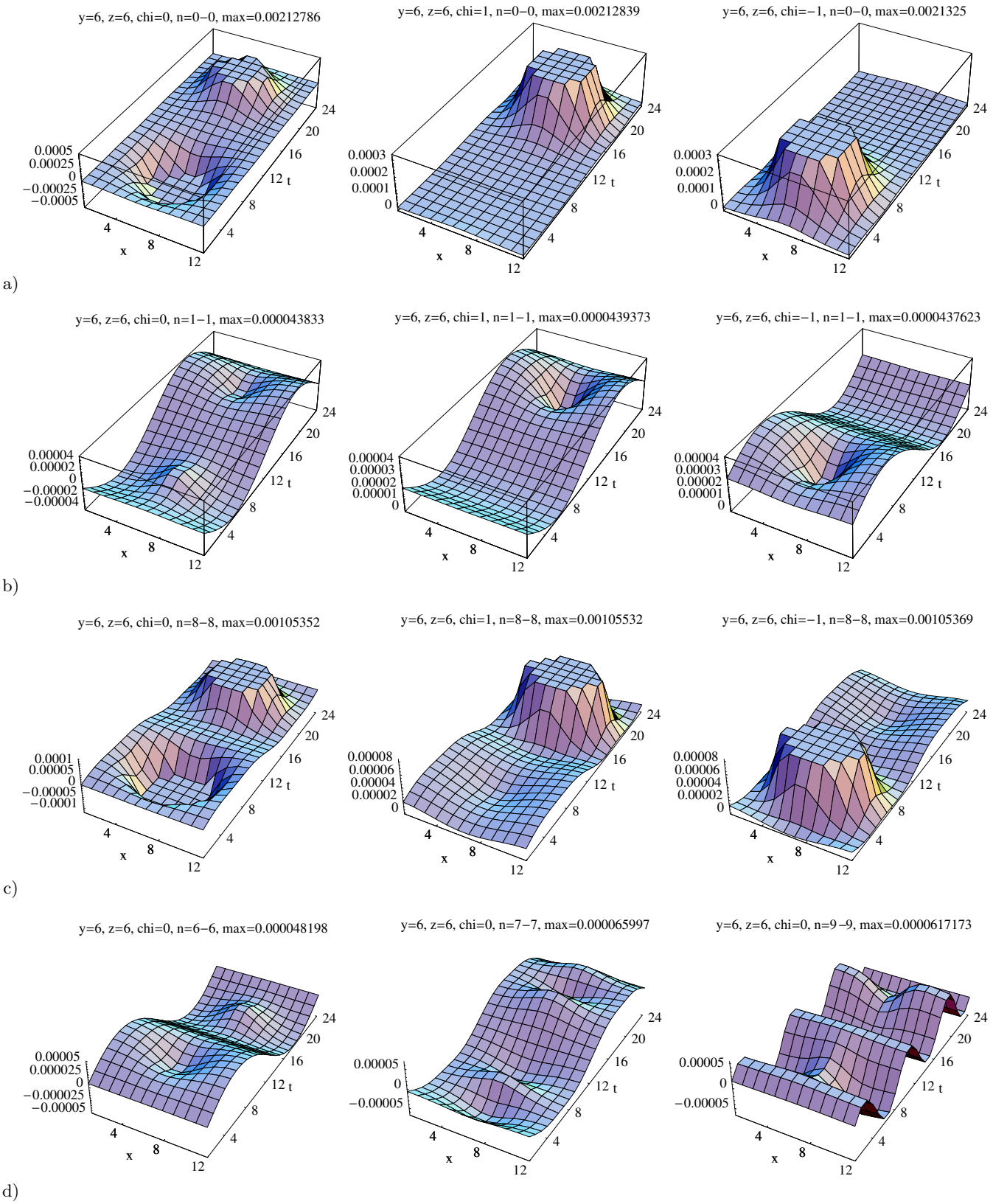

FIG. 6. Chiral densities (ρ_5 left, ρ_- center and ρ_+ right column) of the a) lowest (near-zero), b) second-lowest (nonzero) and c) eighth (nonzero) eigenmode of the overlap Dirac operator for an instanton–anti-instanton pair. d) ρ_5 of the sixth (left), seventh (center) and ninth (right) eigenmode.

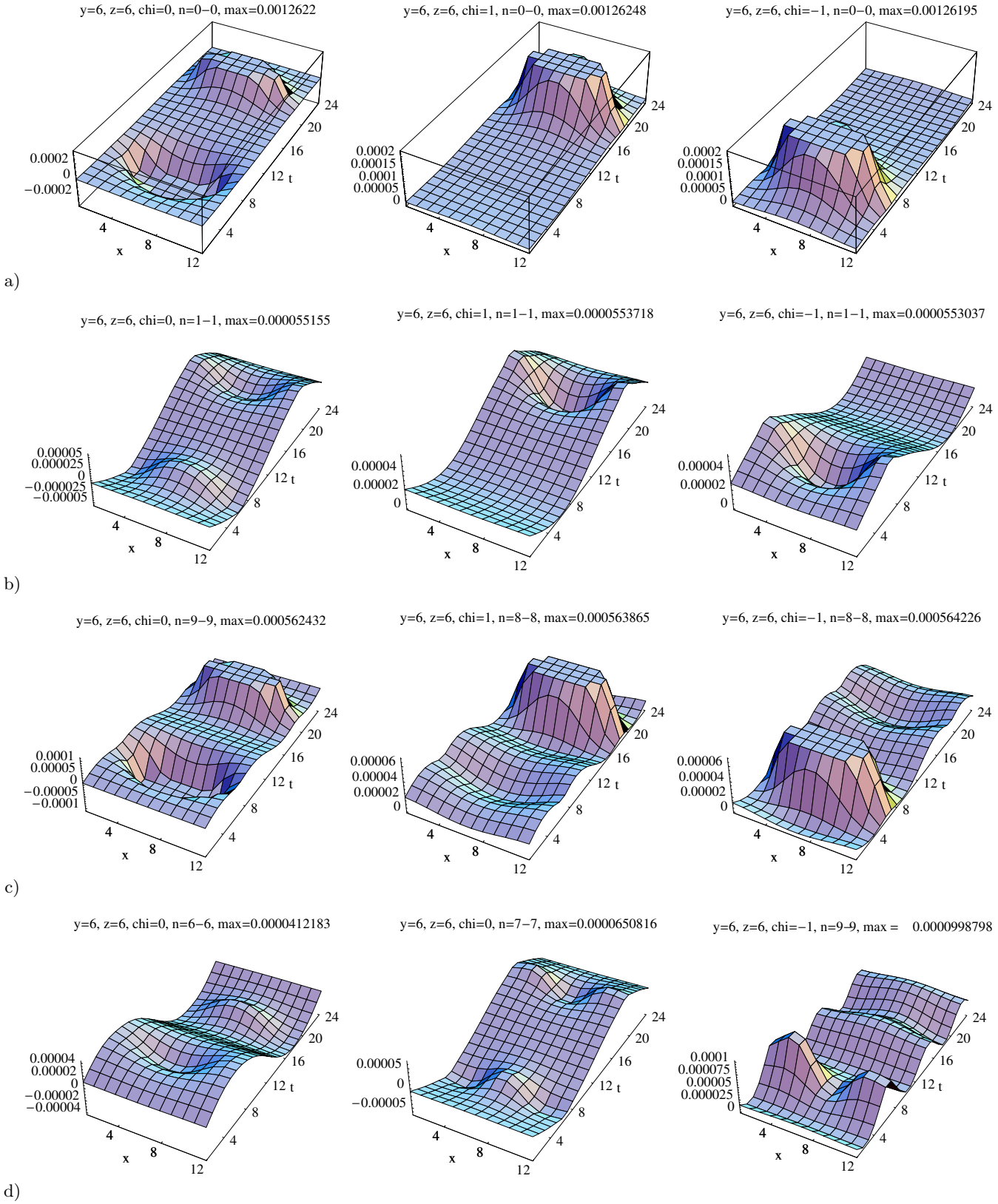

FIG. 7. Same as Fig. 6 but for a spherical vortex-antivortex pair. Chiral densities (ρ_5 left, ρ_+ center and ρ_- right column) of the a) lowest (near-zero), b) second-lowest (nonzero) and c) eighth (nonzero) eigenmode. d) ρ_5 of the sixth (left), seventh (center) and ninth (right) eigenmode.

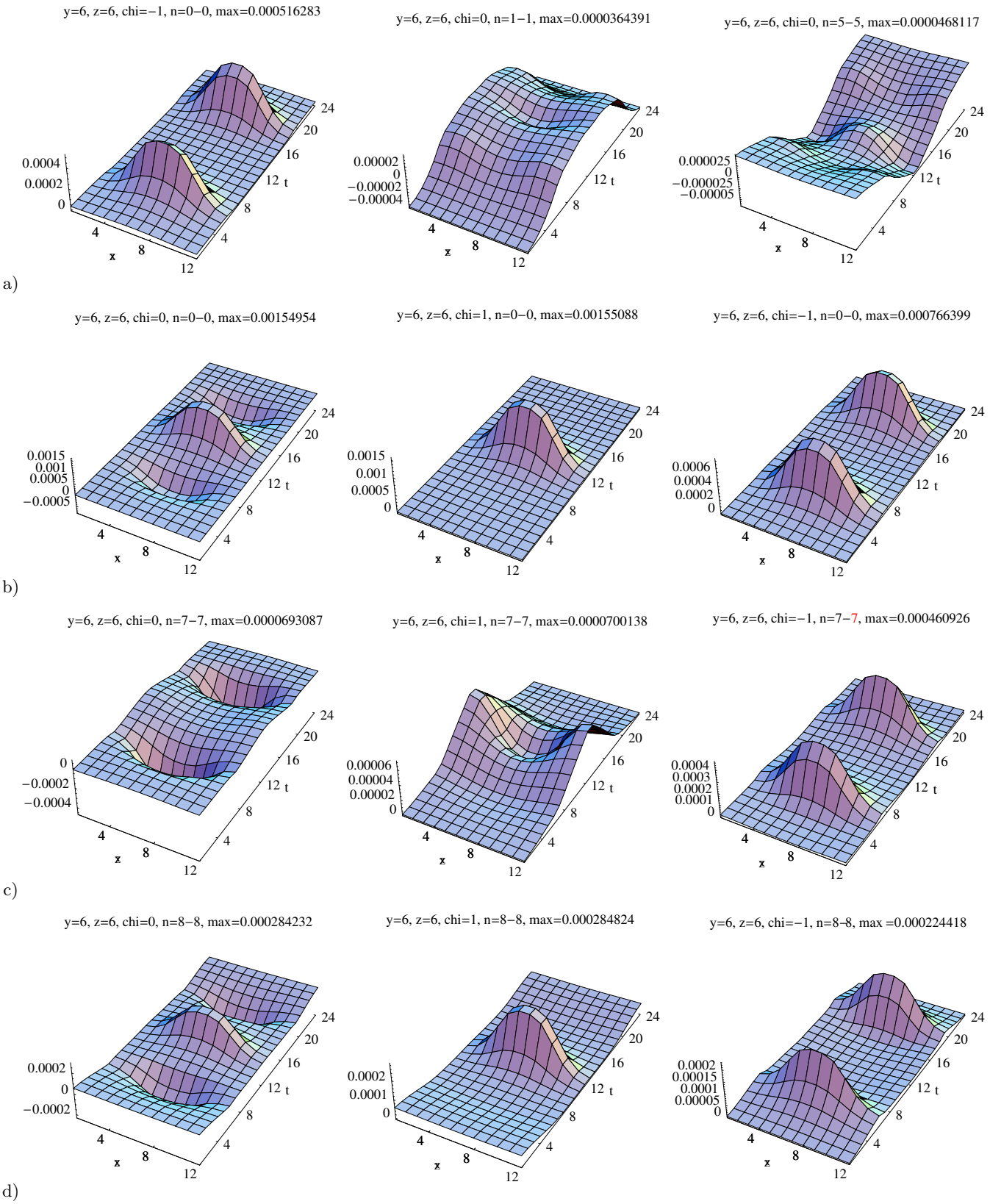

FIG. 8. Chiral densities of overlap eigenmodes for spherical vortices at $t = 4$ and $t = 20$ and an antivortex at $t = 12$: a) zero mode $\rho_-\#0-$ (left), $\rho_5\#1$ (center) and $\rho_5\#5$ (right). b) near-zero (second-lowest) mode #0, c) #7 ($\approx$ #0−) and d) #8 ($\approx$ #0) with ρ_5 (left), ρ_+ (center) and ρ_- (right).

B. Planar vortex configurations

From Sec. III C and Reinhardt *et al.* [48] we recall that plane vortices attract zero modes according to their magnetic flux. For a single pair of parallel vortex slices with the same flux direction we may get two zero modes, peaking at the two vortex slices with the same (local) chirality, see Fig. 10a. But in four dimensions they can be removed by antiperiodic boundary conditions in perpendicular directions of the vortex flux. However, if we intersect two such vortex pairs orthogonally, we get two real zero modes, which we analyzed in [34]. Now, for pairs of (anti)parallel vortex slices with opposite flux directions the situation is similar, except that we only get near-zero modes, it is not clear though how to split them into would-be zero modes. For a single vortex pair we get four near-zero modes peaking at the two vortex slices with opposite (local) chirality, see Fig. 10b. The nonzero modes again show plane wave oscillations, see Fig. 10c. If we intersect antiparallel vortex pairs orthogonally we get two intersection points with topological charge $Q = +1/2$ and two intersection points with topological charge $Q = -1/2$. For such a configuration we get four real near-zero modes, with local chirality peaks at the intersection points, according to their topological charge contribution, see Fig. 9b. Again, the near-zero modes cannot be split into would-be zero modes which could be assigned to single vortex intersections, but the modes rather peak at all intersection points. Hence, the mechanism of Sec. V A does not apply in this case, since there are no localized lumps of topological charge $Q = \pm 1$. Nevertheless the vortices attract chiral near-zero modes via their intersections with topological charge $Q = \pm 1/2$. We expect that vortex intersections, writhing points and even color structure contributions of vortices to topological charge are able to create a finite density of near-zero modes and break chiral symmetry via the Banks-Casher relation.

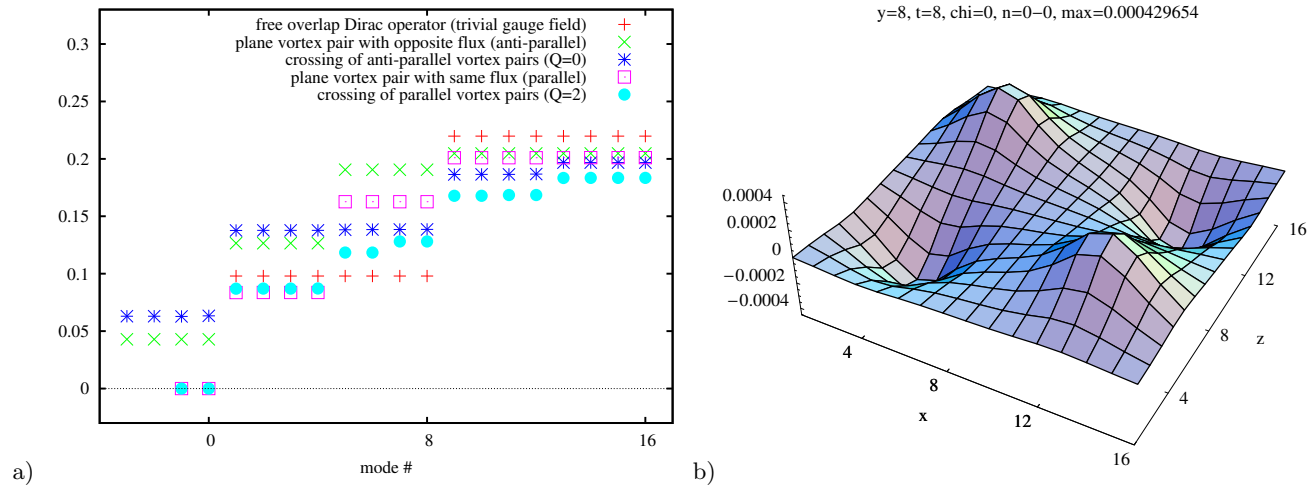

FIG. 9. a) The lowest overlap eigenvalues for plane vortex configurations compared to the eigenvalues of the free (overlap) Dirac operator (red crosses). b) Chiral density $\rho_5 \# 0$ in the intersection plane of four near-zero modes of crossing flat vortex pairs with opposite flux direction ($Q = 0$).

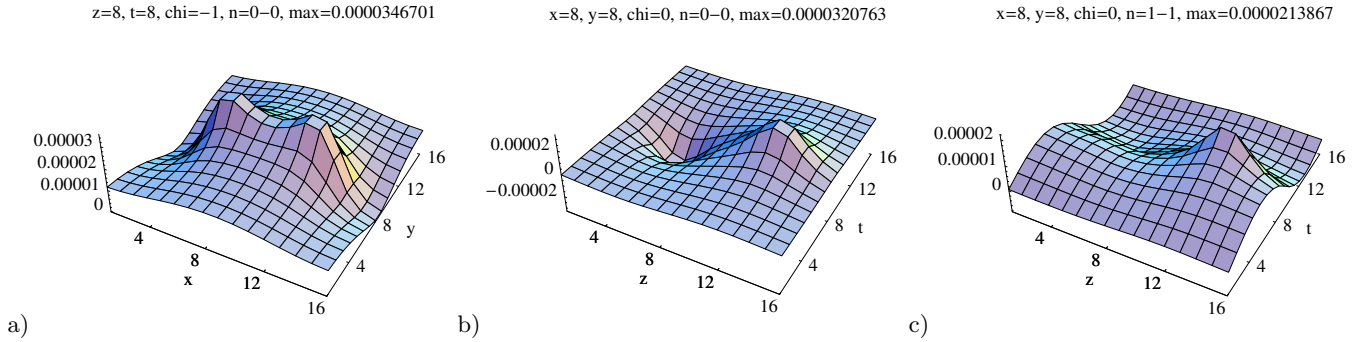

FIG. 10. Chiral densities of the low-lying eigenmodes of the overlap Dirac operator: a) two zero modes of one plane vortex pair, *i.e.*, two vortex slices with the same flux direction, b) four near-zero modes of one plane vortex pair, *i.e.*, two vortex slices with opposite flux direction and c) first nonzero mode of the crossing flat vortex pairs in Fig. 9b).

C. Asqtad Staggered Modes

For completeness we shortly discuss the asqtad staggered eigenmodes for the presented configurations. In principle the same conclusions as for overlap modes apply if we consider the double degeneracy of asqtad staggered modes due to charge conjugation. Hence we have two (would-be) zero modes for $Q = \pm 1$ and there are four times as many near-zero modes since two would-be zero modes do result in two near-zero modes instead of one for overlap modes. We further plot the chirality $\langle \psi \gamma_5 \psi \rangle$ of the asqtad staggered eigenmodes, where γ_5 corresponds to a displacement along the diagonal of a hypercube. To ensure gauge invariance the product includes gauge field multiplications along all shortest paths connecting opposite corners of the hypercube. Staggered fermions do not have exact zero modes, but a separation between would-be zero modes and nonchiral modes is observed for improved staggered quark actions [49]. The plots show that the would-be and near-zero modes have enhanced chirality compared to nonzero modes and we even observe the local chiral density properties for the near-zero modes which we discussed for the overlap modes.

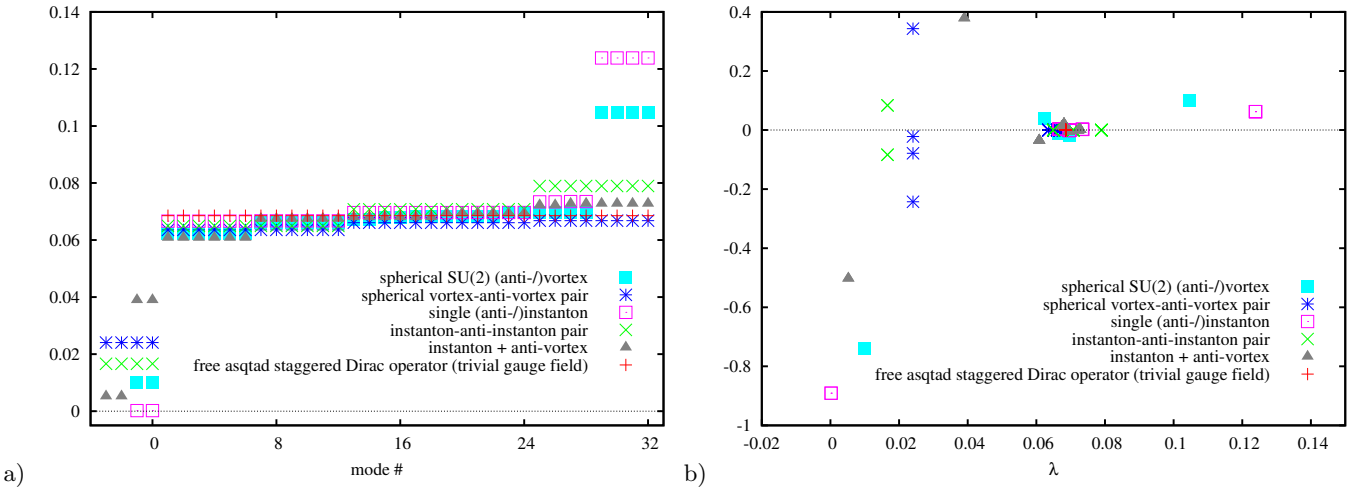

FIG. 11. The lowest asqtad staggered eigenvalues for instanton and spherical vortex configurations compared to the eigenvalues of the free Dirac operator. b) Chirality of the corresponding eigenmodes.

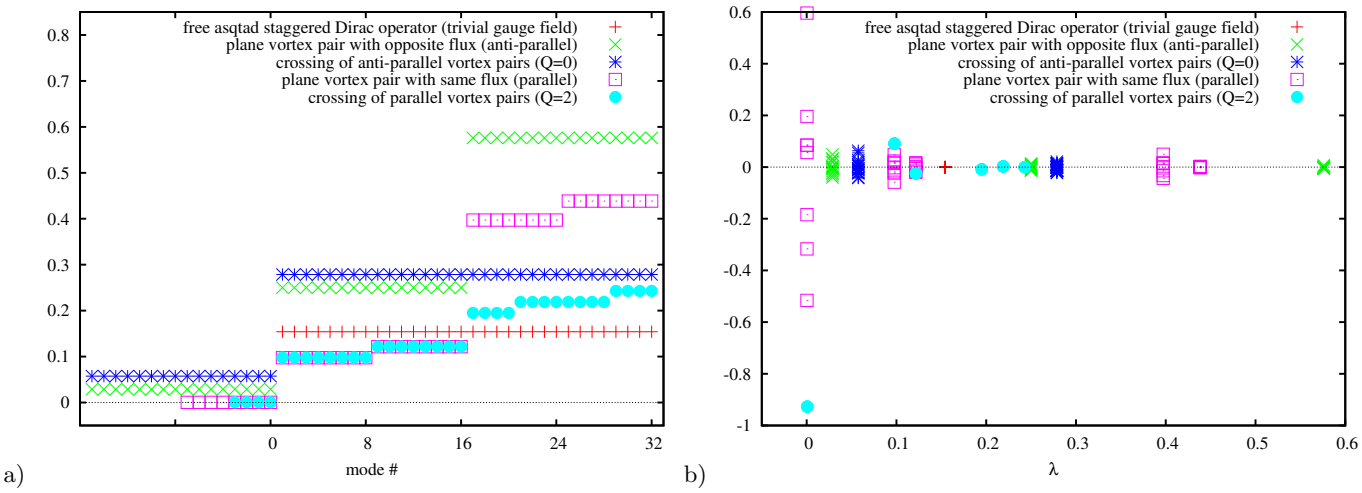

FIG. 12. a) The lowest asqtad staggered eigenvalues for plane vortex configurations compared to the eigenvalues of the free Dirac operator. b) Chirality of the corresponding eigenmodes.

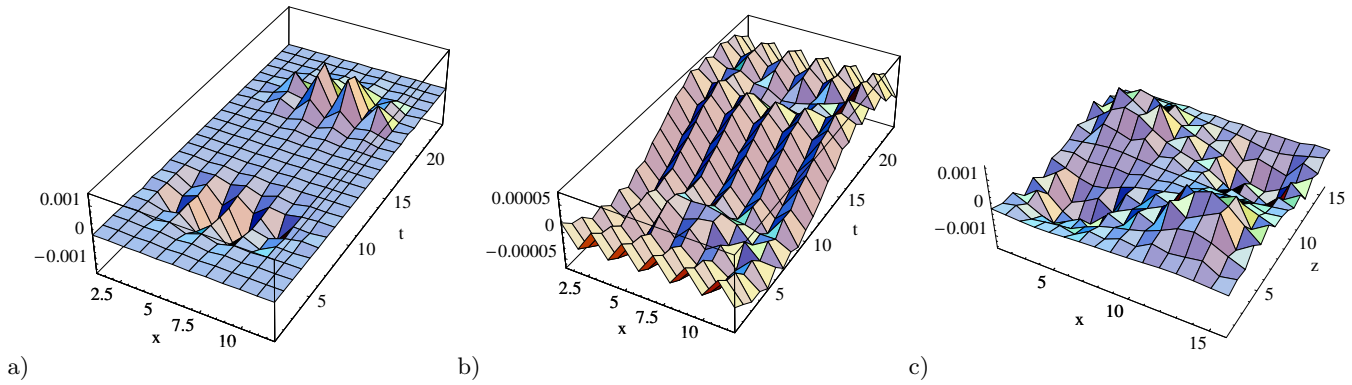

FIG. 13. Chiral densities of the low-lying eigenmodes of the asqtad staggered Dirac operator: a) four near-zero and b) non-zero modes of a spherical vortex-antivortex pair, and c) 16 near-zero modes of the crossing flat vortex pairs in Fig. 9b).

VI. CONCLUSIONS

The instanton liquid model provides a physical picture of chiral symmetry breaking via the idea of quarks hopping between random instantons and anti-instantons, changing their helicity each time. This process can be described by quarks propagating between quark-instanton vertices. As fermions do not seem to make much of a difference between instantons and spherical vortices this picture can be extended to colorful spherical center vortices. But in the vortex picture the model of chiral symmetry breaking can be formulated even more generally, as we have shown that various shapes of vortices attract (would-be) zero modes which contribute via interactions to a finite density of near-zero modes with local chiral properties, *i.e.*, local chirality peaks at corresponding topological charge contributions. The simple picture of localized would-be zero modes from the instanton liquid model or spherical vortex configurations as discussed in Sec. IV and V A does not apply directly to general vortex structures as there are not only topological charge contributions of $Q = \pm 1$. In Monte Carlo configurations we do not, of course, find perfectly flat or spherical vortices, as one does not find perfect instantons. The general picture of topological charge from vortex intersections, writhing points and even color structure contributions or instantons can provide a general picture of χSB: any source of topological charge can attract (would-be) zero modes and produce a finite density of near-zero modes leading to chiral symmetry breaking via the Banks-Casher relation. Here one also has to ask what could be the dynamical explanation of χSB. We can try the conjecture that only a combination of color electric and magnetic fields leads to χSB, electric fields accelerating color charges and magnetic fields trying permanently to reverse the momentum directions on spiral shaped paths. Such reversals of momentum keeping the spin of the particles should especially happen for very slowly moving color charges. Alternatively we could argue that magnetic color charges are able to flip the spin of slow quarks, *i.e.* when they interact long enough with the vortex structures.

Finally, it seems that vortices not only confine quarks into bound states but also change their helicity in analogy to the instanton liquid model. In accordance with Casher's argument, a force strong enough to confine quarks is also generally expected to break chiral symmetry [50], we therefore conclude that the center vortex model of quark confinement may indeed be capable of describing chiral symmetry breaking. We cannot give a conclusive answer to the question of a dynamical explanation for the mechanism of χSB and only speculate on the importance of our results for Monte Carlo configurations, since there vortices are neither perfectly flat nor spherical, as there are no perfect instantons either. But the importance of the long-range nature of low-dimensional topological structures for the understanding of the mechanism of χSB in QCD was underlined by various results of different groups [51–57], and agrees well with a vortex picture of χSB.

ACKNOWLEDGMENTS

We thank Štefan Olejník and Michael Engelhardt for helpful discussions. This research was supported by the Austrian Science Fund FWF ("Fonds zur Förderung der wissenschaftlichen Forschung") under Contract No. P22270-N16 (R.H.).

[1] A. A. Belavin, A. M. Polyakov, A. S. Schwartz, and Y. S. Tyupkin, "Pseudoparticle solutions of the Yang-Mills equations," *Phys. Lett.* **B59** (1975) 85–87.

[2] A. Actor, "Classical Solutions of SU(2) Yang-Mills Theories," *Rev. Mod. Phys.* **51** (1979) 461.

[3] G. 't Hooft, "Computation of the quantum effects due to a four- dimensional pseudoparticle," *Phys. Rev. D* **14** (1976) 3432–3450.

[4] C. W. Bernard, "Gauge zero modes, instanton determinants, and quantum- chromodynamic calculations," *Phys. Rev. D* **19** (1979) 3013.

[5] M. F. Atiyah and I. M. Singer, "The Index of elliptic operators. 5," *Annals Math.* **93** (1971) 139–149.

[6] A. S. Schwarz, "On Regular Solutions of Euclidean Yang-Mills Equations," *Phys. Lett.* **B67** (1977) 172–174.

[7] L. S. Brown, R. D. Carlitz, and C.-k. Lee, "Massless Excitations in Instanton Fields," *Phys. Rev. D* **16** (1977) 417–422.

[8] R. Narayanan and H. Neuberger, "A construction of lattice chiral gauge theories," *Nucl. Phys.* **B443** (1995) 305–385, arXiv:9411108 [hep-th].

[9] E.-M. Ilgenfritz and M. Muller-Preussker, "Statistical Mechanics of the Interacting Yang-Mills Instanton Gas," *Nucl. Phys.* **B184** (1981) 443.

[10] D. Diakonov and V. Y. Petrov, "Chiral Condensate in the Instanton Vacuum," *Phys. Lett.* **B147** (1984) 351–356.

[11] D. Diakonov and V. Y. Petrov, "MESON CURRENT CORRELATION FUNCTIONS IN INSTANTON VACUUM," *Sov.Phys.JETP* **62** (1985) 431–437.

[12] G. 't Hooft, "On the phase transition towards permanent quark confinement," *Nucl. Phys.* **B138** (1978) 1.

[13] P. Vinciarelli, "Fluxon solutions in nonabelian gauge models," *Phys. Lett.* **B78** (1978) 485–488.

[14] T. Yoneya, "Z(n) topological excitations in yang-mills theories: Duality and confinement," *Nucl. Phys.* **B144** (1978) 195.

[15] J. M. Cornwall, "Quark confinement and Vortices in massive gauge invariant QCD," *Nucl. Phys.* **B157** (1979) 392.

[16] G. Mack and V. B. Petkova, "Comparison of Lattice Gauge Theories with gauge groups Z(2) and SU(2)," *Ann. Phys.* **123** (1979) 442.

[17] H. B. Nielsen and P. Olesen, "A Quantum Liquid Model for the QCD Vacuum: Gauge and Rotational Invariance of Domained and Quantized Homogeneous Color Fields," *Nucl. Phys.* **B160** (1979) 380.

[18] L. Del Debbio, M. Faber, J. Greensite, and Š. Olejník, "Center dominance and Z(2) vortices in SU(2) lattice gauge theory," *Phys. Rev. D* **55** (1997) 2298–2306, arXiv:9610005 [hep-lat].

[19] T. G. Kovacs and E. T. Tomboulis, "Vortices and confinement at weak coupling," *Phys. Rev. D* **57** (1998) 4054–4062, arXiv:9711009 [hep-lat].

[20] P. de Forcrand and M. D'Elia, "On the relevance of center vortices to QCD," *Phys. Rev. Lett.* **82** (1999) 4582–4585, arXiv:9901020 [hep-lat].

[21] C. Alexandrou, P. de Forcrand, and M. D'Elia, "The role of center vortices in QCD," *Nucl. Phys.* **A663** (2000) 1031–1034, arXiv:9909005 [hep-lat].

[22] H. Reinhardt and M. Engelhardt, "Center vortices in continuum yang-mills theory," in *Quark Confinement and the Hadron Spectrum IV*, W. Lucha and K. M. Maung, eds., pp. 150–162. World Scientific, 2002. arXiv:0010031 [hep-th].

[23] M. Engelhardt, "Center vortex model for the infrared sector of Yang-Mills theory: Quenched Dirac spectrum and chiral condensate," *Nucl.Phys.* **B638** (2002) 81–110, arXiv:0204002 [hep-lat].

[24] V. Bornyakov *et al.*, "Interrelation between monopoles, vortices, topological charge and chiral symmetry breaking: Analysis using overlap fermions for SU(2)," *Phys. Rev. D* **77** (2008) 074507, arXiv:0708.3335 [hep-lat].

[25] R. Höllwieser, M. Faber, J. Greensite, U.M. Heller, and Š. Olejník, "Center Vortices and the Dirac Spectrum," *Phys. Rev. D* **78** (2008) 054508, arXiv:0805.1846 [hep-lat].

[26] G. Jordan, R. Höllwieser, M. Faber, U.M. Heller, "Tests of the lattice index theorem," *Phys. Rev. D* **77** (2008) 014515, arXiv:0710.5445 [hep-lat].

[27] R. Höllwieser, M. Faber, U.M. Heller, "Lattice Index Theorem and Fractional Topological Charge," arXiv:1005.1015 [hep-lat].

[28] R. Höllwieser, M. Faber, U.M. Heller, "Critical analysis of topological charge determination in the background of center vortices in SU(2) lattice gauge theory," *Phys. Rev. D* **86** (2012) 014513, arXiv:1202.0929 [hep-lat].

[29] T. Schweigler, R. Höllwieser, M. Faber, and U.M. Heller, "Colorful SU(2) center vortices in the continuum and on the lattice," *Phys. Rev. D* **87** (2013) 054504, arXiv:1212.3737 [hep-lat].

[30] H. Reinhardt, "Topology of center vortices," *Nucl. Phys.* **B628** (2002) 133–166, arXiv:0112215 [hep-th].

[31] R. Bertle, M. Faber, J. Greensite, and Š. Olejník, "The structure of projected center vortices in lattice gauge theory," *JHEP* **03** (1999) 019, arXiv:9903023 [hep-lat].

[32] J. Greensite, "The confinement problem in lattice gauge theory," *Prog. Part. Nucl. Phys.* **51** (2003) 1, arXiv:0301023 [hep-lat].

[33] M. Chernodub, F. Gubarev, M. Polikarpov, and V. I. Zakharov, "Monopoles and confining strings in QCD," arXiv:0103033 [hep-lat].

[34] R. Höllwieser, M. Faber, U.M. Heller, "Intersections of thick Center Vortices, Dirac Eigenmodes and Fractional Topological Charge in SU(2) Lattice Gauge Theory," *JHEP* **1106** (2011) 052, arXiv:1103.2669 [hep-lat].

[35] M. Engelhardt and H. Reinhardt, "Center projection vortices in continuum Yang-Mills theory," *Nucl. Phys.* **B567** (2000) 249, arXiv:9907139 [hep-th].

[36] T. M. W. Nye and M. A. Singer, "An L^2-Index Theorem for Dirac Operators on $S^1 * R^3$," arXiv:0009144 [math].

[37] E. Poppitz and M. Unsal, "Index theorem for topological excitations on $R^3 * S^1$ and Chern-Simons theory," *JHEP.* **0903** (2009) 027, arXiv:0812.2085 [hep-th].

[38] T. Schweigler, "Topological objects and chiral symmetry breaking in QCD," Master's thesis, Vienna University of Technology, 2012.

[39] T. Banks and A. Casher, "Chiral Symmetry Breaking in Confining Theories," *Nucl. Phys.* **B169** (1980) 103.

[40] R. G. Edwards, U. M. Heller, and R. Narayanan, "A study of practical implementations of the overlap-Dirac operator in four dimensions," *Nucl. Phys.* **B540** (1999) 457–471, arXiv:9807017 [hep-lat].

[41] R. G. Edwards, U. M. Heller, and R. Narayanan, "A study of chiral symmetry in quenched QCD using the overlap-Dirac operator," *Phys. Rev. D* **59** (1999) 094510, arXiv:9811030 [hep-lat].

[42] B. Bunk, K. Jansen, M. Luscher, and H. Simma *DESY Report* (September 1994) (unpublished).

[43] T. Kalkreuter and H. Simma, "An Accelerated conjugate gradient algorithm to compute low lying eigenvalues: A Study for the Dirac operator in SU(2) lattice QCD," *Comput.Phys.Commun.* **93** (1996) 33–47, arXiv:9507023 [hep-lat].

[44] D. Diakonov, "Instantons at work," *Prog.Part.Nucl.Phys.* **51** (2003) 173–222, arXiv:0212026 [hep-ph].

[45] I. Horvath *et al.*, "Local chirality of low-lying Dirac eigenmodes and the instanton liquid model," *Phys. Rev. D* **66** (2002) 034501, arXiv:0201008 [hep-lat].

[46] R. G. Edwards and U. M. Heller, "Are topological charge fluctuations in QCD instanton dominated?," *Phys. Rev. D* **65** (2002) 014505, arXiv:0105004 [hep-lat].

[47] T. A. DeGrand and A. Hasenfratz, "Low lying fermion modes, topology and light hadrons in quenched QCD," *Phys. Rev. D* **64** (2001) 034512, arXiv:0012021 [hep-lat].

[48] H. Reinhardt, O. Schroeder, T. Tok, and V. C. Zhukovsky, "Quark zero modes in intersecting center vortex gauge fields," *Phys. Rev. D* **66** (2002) 085004, arXiv:0203012 [hep-th].

[49] K. Y. Wong and R. M. Woloshyn, "Topology and staggered fermion action improvement," *Nucl. Phys. Proc. Suppl.* **140** (2005) 620–622, arXiv:0407003 [hep-lat].

[50] A. Casher, "Chiral Symmetry Breaking in Quark Confining Theories," *Phys. Lett.* **B83** (1979) 395.

[51] I. Horvath, S. Dong, T. Draper, K. Liu, N. Mathur, *et al.*, "Uncovering low dimensional topological structure in the QCD vacuum," *JLAB-THY-02-69* (2002) 312–314, arXiv:0212013 [hep-lat].

[52] I. Horvath, S. Dong, T. Draper, F. Lee, K. Liu, *et al.*, "Low dimensional long range topological structure in the QCD vacuum," *Nucl.Phys.Proc.Suppl.* **129** (2004) 677–679, arXiv:0308029 [hep-lat].

[53] P. O. Bowman, K. Langfeld, D. B. Leinweber, A. Sternbeck, L. von Smekal, *et al.*, "Role of center vortices in chiral symmetry breaking in SU(3) gauge theory," *Phys. Rev. D* **84** (2011) 034501, arXiv:1010.4624 [hep-lat].

[54] V. Braguta, P. Buividovich, T. Kalaydzhyan, S. Kuznetsov, and M. Polikarpov, "The Chiral Magnetic Effect and chiral symmetry breaking in SU(3) quenched lattice gauge theory," *Phys.Atom.Nucl.* **75** (2012) 488–492, arXiv:1011.3795 [hep-lat].

[55] E.-A. O'Malley, W. Kamleh, D. Leinweber, and P. Moran, "SU(3) centre vortices underpin confinement and dynamical chiral symmetry breaking," *Phys. Rev. D* **86** (2012) 054503, arXiv:1112.2490 [hep-lat].

[56] P. Buividovich, T. Kalaydzhyan, and M. Polikarpov, "Fractal dimension of the topological charge density distribution in SU(2) lattice gluodynamics," *Phys. Rev. D* **86** (2012) 074511, arXiv:1111.6733 [hep-lat].

[57] V. Braguta, P. Buividovich, T. Kalaydzhyan, and M. Polikarpov, "Topological and magnetic properties of the QCD vacuum probed by overlap fermions," *PoS CONFINEMENT X,* **085** (2013) , arXiv:1302.6458 [hep-lat].